JOURNAL OF Materials CHEMISTRY

Chemical and physical routes for composite materials synthesis: Ag and Ag_2S nanoparticles in silica glass by sol–gel and ion implantation techniques

Lidia Armelao,[a] Renzo Bertoncello,[b] Elti Cattaruzza,[c] Stefano Gialanella,[d] Silvia Gross,*[a] Giovanni Mattei,[e] Paolo Mazzoldi[e] and Eugenio Tondello[a]

[a]*CNR-ISTM and INSTM, Università di Padova - Via Marzolo 1, Padova, Italy. Fax: 0039-049-8275161; E-mail: tilvia@chin.unipd.it*
[b]*Dipartimento di Chimica Inorganica, Metallorganica ed Analitica, Università di Padova - Via Marzolo 1, Padova, Italy*
[c]*INFM, Dipartimento di Chimica Fisica, Università di Venezia - Dorsoduro 2137, Venezia, Italy*
[d]*Dipartimento di Ingegneria dei Materiali, Università di Trento - Via Mesiano 77, Trento, Italy*
[e]*INFM, Dipartimento di Fisica, Università di Padova - Via Marzolo 8, Padova, Italy*

Received 10th April 2002, Accepted 2nd May 2002
First published as an Advance Article on the web 12th June 2002

Two composite systems, "Ag" and "Ag–S" nanoparticles in silica films, were approached by using two different synthesis routes, namely sol–gel and ion implantation. Silica composites containing embedded nanosized silver- and silver sulfide-crystallites were obtained by the sol–gel process. The formation of silver nanograins was also observed in Ag-implanted silica samples, while sequential implantation (first Ag then S) led to the formation of core–shell Ag–Ag_2S nanoclusters. The systems were then characterised using different analytical tools, *i.e.* X-ray photoelectron spectroscopy (XPS), X-ray-excited Auger electron spectroscopy (XE-AES), X-ray diffraction (XRD), secondary-ion mass spectrometry (SIMS), Rutherford backscattering spectrometry (RBS) and transmission electron microscopy (TEM). These advanced microscopic and X-ray analytical methods were combined to gain complementary information concerning the composition and microstructure of the investigated composite systems. In addition, the characterisation of both systems by means of several investigation techniques provided a valuable insight into the potential features offered by sol–gel and ion implantation and enabled a fruitful comparison between these preparative routes. The influence of the different synthesis parameters on the final features of the composites is analysed and discussed.

Introduction

Much scientific and technological interest is nowadays devoted to insulator glasses doped with nanosized crystals of metals or semiconductors, often metal oxides or sulfides, for the development of optical devices with linear and non-linear optical properties.

Nanoclusters represent an intermediate state of matter between discrete molecules and extended-network solids: their properties, due to quantum confinement effects,[1–5] are widely diversified as a function of particle size and geometry.[6] Glass doping with metals or with semiconductor compounds can be performed by methods such as sputtering,[7] ion exchange,[8] ion implantation,[8,9] chemical bath deposition,[10] thermal and electron beam deposition,[11] multitarget magnetron sputtering[12] and by inclusion of pre-formed colloids in a matrix during the gelation process.[11–13]

In this work, two so-called "bottom-up" approaches, namely sol–gel and ion implantation, were adopted to prepare composites formed by Ag or Ag_2S nanoparticles embedded in glassy silica matrices. Both these approaches enable thermodynamic restrictions to be overcome, resulting in material properties unattainable by many other processes.

Silver clusters in silica are of particular interest because their presence enhances the third-order optical non-linear susceptibility of the glass matrix.[1,14] Such nonlinearity leads to an intensity-dependent refractive index, thus allowing the planning and the development of all-optical switching devices. Ag_2S is a semiconductor compound; owing to its intrinsic properties, narrow band gap, easy preparation and good chemical stability, it is usually used for the manufacturing of optical and electronic devices, such as photovoltaic cells, photoconductors, IR detectors[15,16] and superionic conductors.[17] As for metal nanoclusters, the embedding of semiconductor nanosized particles in dielectric matrices leads to composite materials with non-linear optical effects.

The aim of this work is to provide a detailed investigation of these composite systems and to get a meaningful insight into the advantages and drawbacks of the two synthesis techniques. Within this framework, we try to provide answers to the following questions, namely "whether" and "to what extent" the described routes and the related experimental parameters enable a careful control over the final composition and microstructure of the composite materials. To this aim, the comparison focused on two identical systems, "Ag" and "Ag–S", approached through different routes, provided useful indications regarding the effects of the involved experimental parameters on the features of the final nanosystems.

Background to the synthesis techniques

The sol–gel method

The use of the sol–gel technique for the synthesis of oxide-based materials[18,19] is currently attracting much attention. A peculiar feature of the sol–gel process is the ability to go all the

way from molecular source precursors to target product, thus allowing a better control of the whole process and the synthesis of "tailor-made" materials.[20] The chemistry of the sol–gel process is mainly based on hydrolysis and polycondensation of metal alkoxides to form extended networks with an oxide skeleton. Depending on the chemical conditions under which such compounds are polymerised, very different structures ranging from colloidal particles to randomly branched polymers can be obtained. This variability arises from the many different ways in which monomers can be linked and organised when they are in a solvent.[21] The starting precursor solution becomes a sol after the formation of fine colloidal particles or polymers and further reactions lead to gelation, *i.e.* wet gel formation. In the course of *sol-to-gel* conversion, which takes place at low temperatures, coating, fiber drawing and moulding into bulk shapes can be achieved. Among these shapes, films are the most important products of the method. The coating of glass, ceramic, metal and plastic substrates by the sol–gel route is very useful for modifying the properties of substrates or for providing them with active properties to develop new optical, electronic and chemical devices.[22] Moreover, the sol–gel process, with its associated mild conditions, offers new paths for the synthesis of composite materials with domain sizes approaching the molecular level.

Ion implantation

Ion implantation allows the near-surface composition of the implanted solid to be modified independently of the thermodynamic constraints. Ion implantation is a non-equilibrium process: it is possible to dope materials with impurities to concentration levels which far exceed the solubility limits. Moreover, ion implantation can be exploited to design waveguiding structures along prescribed patterns. Both nuclear and electronic processes give rise to structural changes in ion-implanted materials, and several examples of cluster formation of metal atoms implanted in glass matrices are reported in the literature (for a comprehensive review, see refs. 1, 9, and 14). Thus, the doping process is accompanied by precipitation of the implanted species to form nanoclusters, and/or by the formation of new chemical compounds involving both the implanted and the host matrix atoms. The in-depth distribution of the implanted element(s) is quite easily predictable by means of simulation software packages, such as the TRIM code[23] and the DYNA code,[24] being mainly determined by the ion beam energy and by the mass of both the incident ions and of the atoms of the solid target. Some differences between the predicted depth profile and the experimental one may take place due to diffusion of species during the implantation (radiation-enhanced diffusion, RED). In view of these characteristics, ion implantation exhibits a large synthesis versatility, leading to both metastable and equilibrium phase formation. However, the composition attainable by ion implantation may be limited by sputtering effects induced by the implantation process itself. As far as the nanocluster formation is concerned, the chemical reactivity of the species involved in the ion implantation process comes into play both in the growth and in the structure of the nanoparticles.[25] The physical mechanisms governing cluster formation are still under debate, even for single metal implants.[8] In general, thermodynamic considerations in terms of Gibbs energy variation allow some raw predictions to be made about the possible resulting aggregate, but the proposed models are still only partially effective.[9] Recently, a kinetic 3D lattice Monte-Carlo model was proposed[26] to study the diffusion, the precipitation and the interaction kinetics of sequentially implanted elements in a chemically neutral matrix. This simulation, applying a simplified model of collision mixing, gives an indication of whether the formation of single-element or more complex structures (as core–shell, alloy or compound clusters) are favoured, by comparison of the nearest-neighbour bond strengths of the different compounds.

Experimental

Ag- and Ag_2S-silica composite systems

For both synthesis routes, Herasil silica slides, 15 × 25 × 1 mm, supplied by Hereaus, were used as substrate.

The main difference between the two synthesis techniques is the way of introducing the guest species to the host material. Usually, in ion implantation the target of the impinging ions is a solid matrix in which ions are implanted using energy ranging between 5 and 100 keV. Conversely, in the adopted sol–gel approach, the gelation and formation of the host matrix as well as the nucleation and growth of the guest particles occur simultaneously.

Experimental details

The synthesis and characterisation of the investigated systems are extensively described in the references quoted in Table 1. Table 1 summarises also the labels by which the four studied samples will be referred to in the text.

For the implanted samples, the substrate temperature never exceeded 330 K during irradiation. Implanted films were obtained by using the experimental conditions outlined in detail in Table 1.

Sol–gel films were obtained by the dip-coating procedure. Before use, the silica slides were cleaned and rinsed both in doubly distilled water and isopropyl alcohol. This procedure, repeated several times, aims at removing organic residues from the surface and at favouring the best adhesion between coating and substrate. Slides were finally dried in air at room temperature. Film deposition was carried out in air, at room temperature, with a withdrawal speed of 10 cm min^{-1}. A volume of about 20 ml solution was used for the dipping. As concerns the Ag(sg) and Ag–S(sg) systems, the as-prepared samples contained only silver ions and the silver–thiourea complex, respectively. Such species evolved into metallic silver and silver sulfide particles as a consequence of thermal annealing. Since the nanosized particles form inside a highly viscous matrix, the growth and size distribution of the clusters can be controlled and tailored. As a matter of fact, in the synthesis of these

Table 1 Experimental routes for the preparation of the four investigated samples and labels adopted in the text

Sample label	Ref.	Synthesis route
Ag(ii)	27	Ion implantation of Ag^+ ions (270 keV) with different fluences (5 or 6 × 10^{16} atom cm^{-2}) and current densities (1.0 or 1.5 μA cm^{-2}), at room temperature
Ag–S(ii)	28	Ion implantation of Ag^+ (65 keV, 5 × 10^{16} atom cm^{-2}, 1.5 μA cm^{-2}) and S^+ (30 keV, 2 × 10^{16} atom cm^{-2}, 1.5 μA cm^{-2}) ions with different implantation sequence, at room temperature
Ag(sg)	29	Sol–gel synthesis of Ag clusters from silver acetate and amino-silane and thermal treatments
Ag–S(sg)	30	Sol–gel synthesis of Ag_2S clusters from thiourea, TEOS and silver acetate and thermal treatments

metal- or semiconductor-doped silica coatings, two main aspects were taken into account: the purity of the films and an accurate control over particle size and distribution.

For the Ag(sg) system, in order to prevent the uncontrolled formation of metal particles in the starting solution and the inclusion of contaminants (*i.e.* inorganic anions) in the prepared coatings, the amino-functionalized silane compound $(CH_3O)_3Si(CH_2)_3NH(CH_2)_2NH_2$ and silver acetate (CH_3COOAg) were used as precursors for the silica network and the metallic phase, respectively. As a matter of fact, the use of a *single-source* precursor in which the silane part originating the silica glassy matrix is combined with amino ligand groups able to "anchor" the silver ions, allows the simultaneous formation of the host network and of the guest nanoparticles, at the same time enabling an effective control over the particle size and distribution. As extensively discussed in the following, a homogeneous particle distribution was evidenced by the TEM analyses.

Alcoholic solutions containing the precursors were prepared as outlined in the following.

For Ag(sg) samples, isopropyl alcohol (C_3H_7OH) was used as solvent. The silane precursor for the silica matrix was *N*-[3-(trimethoxysilyl)propyl]ethylendiamine. Just before use it was purified under vacuum distillation (10^3 Pa, 135–140 °C) and stored under an argon atmosphere. Silver was introduced as silver acetate in solution. The choice was made taking into account that under heating acetate decomposes more easily with respect to other inorganic compounds, without leaving residual contaminants inside the coatings. Besides these precursor compounds, water and acetic acid (CH_3COOH) were added to the solution, so that hydrolysis occurred in acidic conditions. The molar ratios of the components in the solution were isopropyl alcohol/silane = 10 : 1, water/silane = 4 : 1 and acetic acid/silane = 0.6 : 1, while the atomic ratio of Ag to Si was 0.16 : 1. The addition sequence was the following. Firstly, CH_3COOAg was dissolved in the silane and successively, isopropyl alcohol, water and acetic acid were added. The precursor solution was heated at 60 °C for 3 h and underwent aging for two days before use for the film deposition.

In the case of Ag–S(sg) films, attention was focused on the synthesis of a compound containing Ag–S bonds which was to be used as precursor for the silver sulfide clusters. CH_3COOAg was employed as the silver salt. Thiourea, which is well known as being an effective silver ion complexing ligand, was used as the sulfur source. A colourless, transparent and stable solution (A) of silver sulfide precursors was obtained by dissolving silver acetate and 1,3-diethyl-2-thiourea in anhydrous ethanol with molar ratios of silver acetate/thiourea/ethanol = 1 : 11 : 14. Acetic acid was added to the solution with ethanol/acetic acid = 12 : 1 molar ratio. A second solution (B), clear, transparent and stable was prepared by dissolving tetraethoxysilane (TEOS) [$Si(OEt)_4$] in ethanol with a TEOS/ethanol molar ratio of 1 : 20. This solution, stirred for 1 h at room temperature, was then partially hydrolysed by adding water and acetic acid in the molar ratio silver acetate/acetic acid/water = 1 : 0.14 : 4.9. The solution was then aged at 60 °C for 10 min. Solutions A and B were then mixed in the weight ratio of 1 : 1.5 and stirred for some minutes at room temperature before use. The obtained films were annealed in nitrogen at temperatures ranging between 200 and 600 °C for one hour. This inert atmosphere was used to avoid the formation of sulfate, which is favoured in oxidative conditions.

The chemical composition of the prepared samples was determined by XPS, XE-AES, SIMS and RBS. Their microstructure was investigated by XRD and TEM. TEM measurements were performed on two different microscopes. TEM_1 analyses used a Philips CM30 T microscope equipped with an EDAX energy dispersive X-ray spectroscopy (EDXS) system and operating at 300 kV at CNR-LAMEL in Bologna (Italy). The TEM_1 samples (cross or planar sections) were obtained with the procedure described in refs. 27–29. TEM_2 observations were conducted on specimens obtained following conventional cutting and mechanical thinning procedures involved with cross-sectional preparation. The final thinning was carried out using a GATAN ion-mill. To reduce any possible heating effects during ion bombardment, a cryogenic, liquid-nitrogen cooled sample holder was used. Edge-on observations were conducted with a Philips 400T instrument operated at 120 kV and equipped with an energy dispersive X-ray spectroscopy (EDXS) system.[30] Further information was obtained by optical absorption spectroscopy.

Results and discussion

Ag systems

Concerning Ag(ii) samples, spherical nanoparticles embedded in silica were obtained in all the investigated implantation conditions. Fig. 1a and 1b report the cross-sectional bright-field images of the samples implanted under "low conditions" (5×10^{16} atom cm^{-2} of fluence and 1.0 μA cm^{-2} of current density) and "high conditions" (6×10^{16} atom cm^{-2} and 1.5 μA cm^{-2}), respectively. Chemical investigation performed by XPS and XE-AES indicates the presence of metallic silver. In particular, since the BE energies of metallic silver and silver oxide are similar, the different silver oxidation states were evaluated by using the Auger α_1 and α_2 parameters, defined as the sum of the BE value of the $Ag3d_{5/2}$ XPS region and the kinetic energies (KE) of the AgM_5NN and the AgM_4NN Auger peaks, respectively. XRD and selected area electron diffraction (SAED) patterns clearly evidence the presence of crystalline silver. The nanoparticles exhibit the same lattice parameters as the bulk silver, and no preferential crystallographic orientation is evidenced. As pointed out by TEM_1 analyses, the in-depth mean cluster size distribution can be symmetric or asymmetric

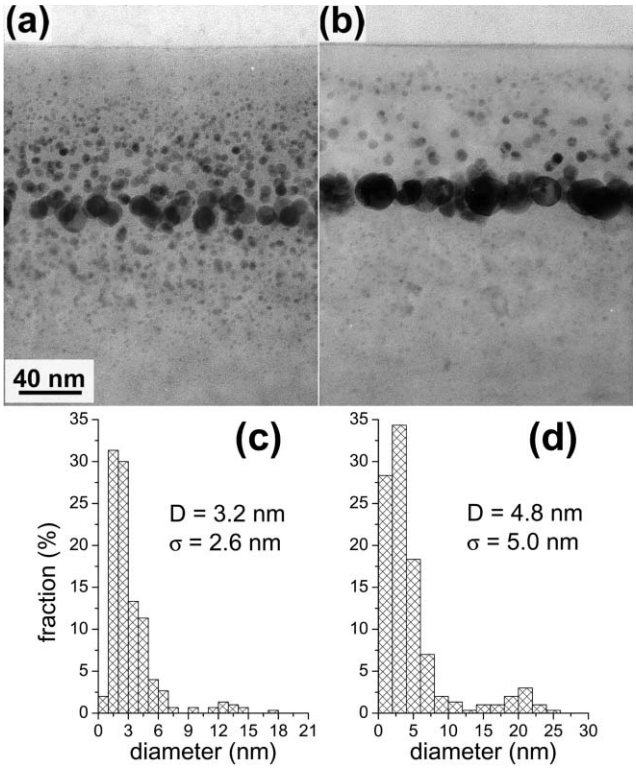

Fig. 1 Bright field TEM_1 cross-section micrographs of Ag(ii) samples: 5×10^{16} atom cm^{-2} of fluence and 1.0 μA cm^{-2} of current density (a); 6×10^{16} atom cm^{-2} of fluence and 1.5 μA cm^{-2} of current density (b); (c) and (d) are the histograms of size distribution for the two samples (a) and (b), respectively. The average diameter and the standard deviation of the experimental distribution are reported.

depending on the experimental parameters, *i.e.* current density and fluence, employed during the implantation process. Although no intensive studies have been carried out, the experimental findings suggest that the higher both the ion current density and the fluence are, the more evident is the formation of silver clusters. Moreover, they also induce the formation of nanoclusters with larger mean diameter value, as can be seen in the histogram of size distribution reported in Fig. 1c and 1d corresponding to the samples in Fig. 1a and 1b, respectively. In both cases, a lognormal size distribution is found with the onset of bimodal distribution as the fluence and current densities are increased. In particular, high current densities seem to favour and enhance the aggregation of the implanted silver atoms: they aggregate to form larger and larger metallic clusters, whose dimension reaches its maximum size (20–25 nm) close to the depth of highest radiation damage (Fig. 1b). Ion current density and fluence affect the features of the final system by inducing variation in the (radiation-enhanced) diffusion, responsible for the mobility of the metal ions inside the matrix and for different precipitation effects. The distribution of silver inside the implanted region is far from being homogeneous, showing a characteristic bimodal shape which is often encountered also for copper ion implantation in silica glass.[31] Starting from the observation of a lattice parameter contraction of the obtained silver nanoclusters, recently Dubiel *et al.*[32] have tried to explain the bimodal in-depth distribution. In silver-implanted soda-lime glasses (at room temperature) this appears as a phenomenon induced by strong compressive stresses existing in implanted glasses at temperatures well below the glass transition one. These compressions would affect both the migration and the aggregation of silver atoms.

In the Ag(sg) system, silver nanocluster precipitation was achieved after thermal annealing. In the sample annealed in air for 1 h at 600 °C, the decomposition of the precursor was complete: in this case the silver clusters are well separated and homogeneously dispersed inside a pure host silica matrix (Fig. 2a). The particle size distribution exhibits a long tail toward large sizes: the mean particle diameter is 4 nm with a standard deviation of the distribution of 3.9 nm (Fig. 2b). High resolution TEM_1 analysis indicates that some of the particles exhibit a faceted shape (Fig. 3). To investigate the thermal evolution of the as-prepared samples, they were annealed in air for 1 h at different temperatures, ranging from 400 °C to 800 °C. XPS and XE–AES showed that the silver oxidation state changes with temperature. In particular, at temperatures up to 550 °C the silver is still partly oxidised (Ag^+), even if the reduced form (Ag^0) is already present. In the 600 °C heated sample, nearly all the silver is present as Ag^0. However, a faint interaction between silver nanoclusters and their chemical environment, *i.e.* the silica matrix, was pointed out by SIMS analysis. Such investigation showed both AgO^+ and $AgOSi^+$ fragments, ascribed to the presence of some oxidised silver

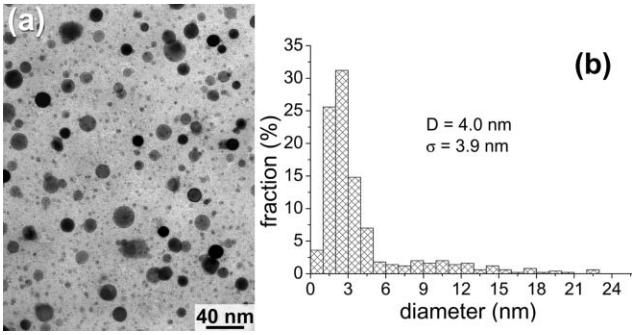

Fig. 2 Bright field TEM_1 planar view micrograph of the Ag(sg) sample annealed in air at 600 °C (a); histogram of the size distribution (b).

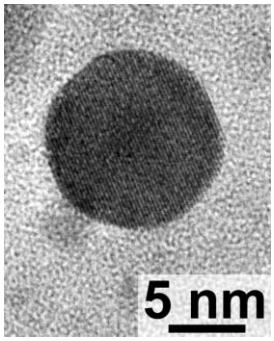

Fig. 3 High resolution TEM_1 micrograph of the Ag(sg) sample annealed in air at 600 °C. The icosahedral shape of the silver nanoparticle is clearly visible, as well as the lattice fringes of the (111) silver planes.

atoms and to the formation of a silicate shell surrounding the nanoclusters.

With respect to higher fluence Ag(ii) implanted samples, for which X-ray and electron diffraction patterns pointed out the formation of crystalline silver in as-implanted samples, in the Ag(sg) samples X-ray diffraction peaks are not detected up to 600 °C. In the 600 °C annealed sample, sharp X-ray diffraction peaks were instead observed. Moreover, the optical absorption spectrum of the sample heated at 600 °C is characterised by a very intense band, peaked at 407 nm and ascribed to the surface plasmon resonance of the silver clusters. For higher temperature annealing treatments in air, the oxidation state of the silver atoms changes abruptly. The 800 °C heated sample appears completely colourless since the Ag^0 atoms undergo a complete oxidation to Ag^+.

Ag–S systems

As concerns the system "Ag–S", the results obtained using ion implantation and sol–gel are remarkably different. The double ion implantation allows the exploitation of the chemical affinity of the two doping elements to obtain nanostructured compounds and/or heterosystems, such as core–shell clusters. As far as the Ag–S(ii) samples are concerned, the sequence of implantation firstly affects the amount of dopants retained in the host matrix, thus modifying the previously estimated local concentration ratio of the two implanted species. The implantation of the second chemical element, *i.e.* sulfur in the case of Ag + S sample and silver in the S + Ag sample, induces a remarkable depletion of the first implanted element, whose resulting concentration is about half the nominal dose. The depletion of the pre-implanted atoms is due to their RED towards the sample surface and to preferential sputtering during implantation. This latter phenomenon, usually more evident for dopant species weakly interacting with the host matrix, represents a limitation since the actual amount of the dopant atoms inside the matrix becomes hardly predictable. Actually, in the S + Ag sample the S retained dose is about 50% of the nominal implantation one (the Ag retained dose is about 90%), while in the Ag + S sample the Ag retained dose is about 60% of the implantation dose (100% for S).

In both Ag–S(ii) samples, TEM_1 revealed the formation of a very large number of nanoparticles embedded in the silica matrix (Fig. 4). In the S + Ag sample we found a cluster diameter distribution characterised by a mean value of 12 nm and a standard deviation of 5 nm; in the Ag + S one we found 9 nm and 5 nm, respectively. SAED patterns indicated that in the S + Ag sample the nanoparticles have the same fcc crystalline structure and lattice parameter as the silver bulk phase (Fig. 5a). In the Ag + S sample, however, the diffraction pattern showed in addition (less intense) spotty rings characteristic of acanthite (Fig. 5b), one of the three crystalline phases of Ag_2S between room temperature and the melting point. Just

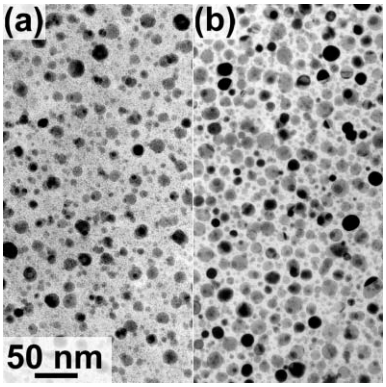

Fig. 4 Bright field TEM_1 planar view micrographs of the Ag–S(ii) samples: first S then Ag ion implantation (a); first Ag then S ion implantation (b).

for comparison, Fig. 5c reports a simulation of the bulk powder diffraction pattern of a mixture of Ag and Ag_2S crystalline phases. In the S + Ag sample, the in-depth cluster distribution showed a bimodal shape, with the largest clusters (with a mean diameter around 10 nm) mainly localised at the surface and at 35 nm depth (Fig. 6a); in the Ag + S sample, the in-depth distribution of cluster dimensions was more uniform (Fig. 6b). This finding can be attributed to the marked RED of silver atoms during sulfur irradiation: the irradiation-induced defects act as nucleation centres for the diffusing silver atoms, leading to the formation of large silver nanoprecipitates in all the irradiated regions.[27]

The TEM_1 cross-sectional micrograph of the Ag + S sample clearly showed that many clusters are characterised by a core–shell structure (Fig. 6b): they have metallic silver cores

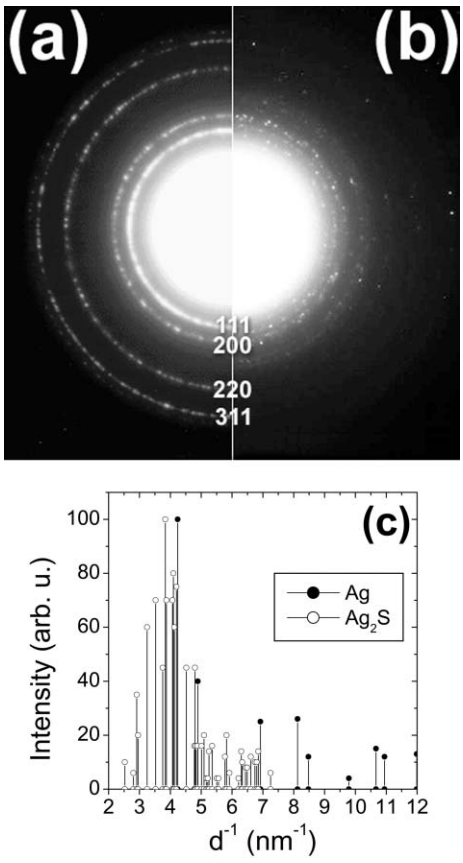

Fig. 5 TEM_1 selected area electron diffraction pattern of Ag–S(ii) samples: first S then Ag ion implantation (a); first Ag then S ion implantation (b); the Miller indexes of the Ag fcc phase are reported; simulation of the diffraction pattern resulting from a two phase system with fcc Ag and acanthite (c).

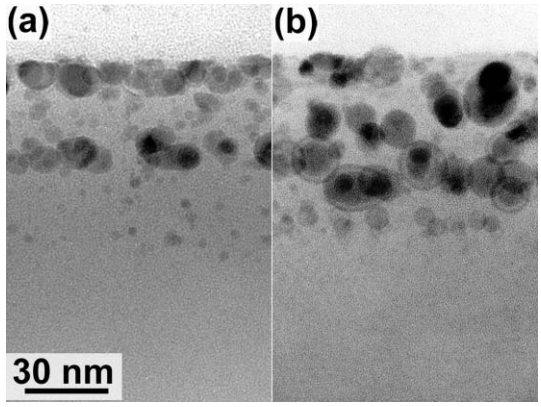

Fig. 6 Bright field TEM_1 cross-section micrographs of Ag–S(ii) samples: first S then Ag ion implantation (a); first Ag then S ion implantation (b).

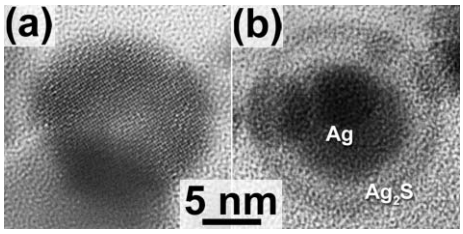

Fig. 7 High resolution TEM_1 micrograph on a core–shell nanoparticle of the silica sample with Ag implantation first then S: lattice fringes of the shell silver sulfide planes (a); bright field view of a nanoparticle, clearly evidencing the core–shell structure (b).

surrounded by silver sulfide crystalline shells (Fig. 7). These crystalline core–shell clusters (hetero-systems) originate only in the deeper implanted regions of the Ag + S sample, where there is a high atomic fraction of sulfur when compared to silver. All these findings suggest that the implantation sequence can be a very important parameter in obtaining particular compounds and/or nanostructures by means of double ion implantation. Moreover, the formation of acanthite, *i.e.* the (bulk) Ag_2S phase stable up to 180 °C, is in agreement with the picture of the ion implantation as a low-temperature physical process[9] if regarded at the time scales characteristic of the thermodynamic and diffusive behaviours.

As suggested by XPS, XE-AES and SIMS data, in the two Ag–S(ii) samples a weak chemical interaction of both silver and sulfur with the host matrix was pointed out. Moreover, sequential ion implantation of silver and sulfur leads also to a (moderate) chemical interaction between the two elements: the formation of a detectable amount of silver sulfide was evidenced. However, the chemical behaviour of silver and sulfur, as well as the chemical and morphological modifications of the sample surface, are affected by the implantation sequence. From a chemical point of view, in the S + Ag sample the interaction between sulfur and silver is slightly stronger than in the Ag + S specimen. From a structural point of view, the formation of a crystalline phase (acanthite) of Ag_2S is detected only in the latter sample, as already described.

In the Ag–S(sg) sample, different analyses lead to the conclusion that silver sulfide clusters embedded in an amorphous silica matrix were obtained. Silver sulfide nanocrystallites were synthesised in the silica matrix starting from solutions containing a thiourea–silver complex where a silver–sulfur interaction is already present. This molecular approach, together with a careful optimisation of the experimental parameters (composition of the solution, time and temperature of ageing, deposition conditions), provides good control over cluster formation. As shown by XRD, the Ag_2S crystallites in the

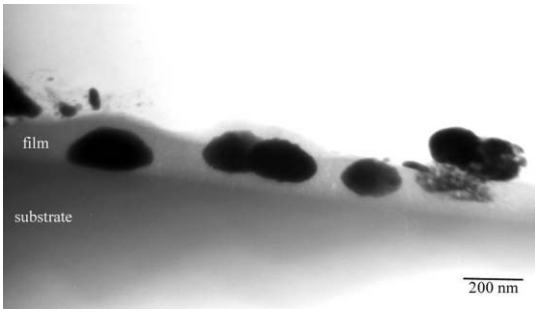

Fig. 8 Cross sectional TEM_2 micrograph of the Ag–S(sg) sample, showing Ag_2S crystals inside the SiO_2 film.

acanthite phase are obtained after the 300 °C thermal treatment and exhibit a mean size of 25–30 nm. These crystallites are supposed to aggregate to give larger clusters. In fact, TEM_2 observation revealed the presence of prolate clusters with a mean size of 200–250 nm, quite homogeneously distributed inside a layer 350 nm thick (Fig. 8). EDXS analyses performed on the same sample revealed that silver and sulfur are mainly localised inside the clusters (Fig. 9), whereas they are nearly undetectable inside the glassy matrix (Fig. 10). This is an indication that the precursors decomposed completely to give silver sulfide crystal aggregates.

Conclusions

Although a systematic investigation is still lacking, currently available data allow us to draw some general conclusions and to point out general trends concerning the Ag–SiO_2 and Ag_2S–SiO_2 systems approached by the two synthesis techniques.

Ion implantation. As far as ion implantation is concerned, even if the exact role of the single experimental parameters is still not clearly understood, both fluence and current density have proved to play a major role in defining the final structure and morphology of the system through the formation of defects in the host matrix. The mean diameter of the precipitates increases and the density decreases with increasing implantation fluence and temperature.[33] Moreover, ion implantation is

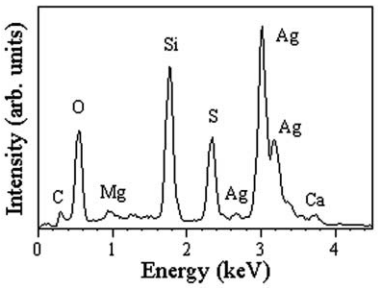

Fig. 9 EDXS spectrum acquired on one of the Ag_2S grains of the Ag–S(sg) sample.

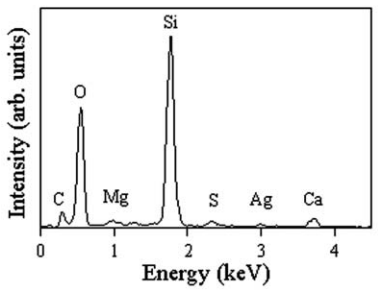

Fig. 10 EDXS spectrum acquired inside the synthesized film of the Ag–S(sg) sample in a crystal-free region.

characterised by a high density of precipitates and one of the most interesting features of implanted samples is the small mean size of the particles. The obtainable cluster size ranges from atomic dimensions up to the thickness of the implanted layer. Anyway, the mean size is not easily controlled since implantation parameters affect the final cluster diameter distribution. Experimental findings support the hypothesis that there is an excess of nucleation sites for new phase formation. This hypothesis is strengthened by two observations. First of all, the density of the precipitates can be much higher than that achieved by other methods. This very high density of small precipitates is related to a remarkable presence of nucleation sites. A high density of nucleation sites is believed to be related to the displacement damage, a consequence of ion implantation. The induced defects probably provide a large number of nucleation sites for new phases. Secondly, the observation of nucleation-limited phenomena in implanted systems has not yet been reported. As already outlined, the retained dose of implanted ions may be markedly lowered by sputtering phenomena. Moreover, due to RED phenomena, to collisional cascades, and to the diffusion trend of certain elements (*e.g.* silver), the actual distribution of guest species inside the implanted region is hardly controlled. The implantation sequence has also proved to play an outstanding role in determining the chemical behaviour of the implanted species. As highlighted by the Ag(ii) systems, the chemical behaviour of the impinging ions is strongly influenced by the chemical environment they find in the target matrix.

Sol–gel. Several process parameters (*i.e.* nature of the precursors, solution composition, atmosphere of deposition, time and temperature of ageing, *etc.*) are involved in determining the features of the final products. On the basis of our experimental evidence, the final morphology of sol–gel derived films is strictly related to the way the guest clusters inside the host matrix were grown. The adopted procedure, combined with a careful thermal treatment, has proved to be very suitable to synthesize silver and silver sulfide nanocrystallites embedded in silica. As the approach employed for the "Ag" system demonstrates, an effective anchoring of the guest species to the building matrix by a proper functionalized silica precursor was attained. Besides promoting an intimate coupling among host matrix and guest species, this approach provides also a powerful method of controlling both the average size of the nucleating clusters and their average size distribution, which is considerably narrowed with respect to other synthesis routes. As a matter of fact, a proper choice of the starting precursors induces nucleation of the guest particles inside the gelling network, thus avoiding a separation in different phases and a subsequent uncontrolled growth of the clusters. Also in the "Ag–S" system, the optimisation of the solution in terms of choice of suitable silver and sulfur sources, molar ratios among the solution components, time and temperature of ageing, allowed the formation of Ag_2S nanocrystallites embedded in a pure silica matrix.

It is worth noting that, while sol–gel allows nanosized silver sulfide particles to be obtained, ion implantation provides a powerful tool to produce core–shell structures. Metal cores coated with a semiconductor layer, due to the unique interface interactions, are attracting a growing interest especially in the field of semiconductor technology.

General remarks. With respect to the sol–gel route, ion implantation allows local concentrations of the dopant elements up to several tens of atomic percentages to be achieved. However, as already mentioned, a careful control on both their in-depth distribution and their size distribution is far from being achieved.

Also the mobility of species inside the host matrix is expected to be quite different. In sol–gel, the presence of a solution in the

early stages of the process up to the gelation point leads to a remarkable mobility of the guest species. In ion implantation (of solid targets) this mobility is markedly lower. Nevertheless, a large amount of structural defects induced by the implanted atom collisional cascades can enhance the dopant atom diffusion. This phenomenon, together with a number of other additional effects leading to deviation in the implanted atom distribution from that expected for simple implantation and diffusion processes, may favour chemical interaction among different implanted elements.

Acknowledgement

This work was partially funded by Progetto Finalizzato "Materiali Speciali per Tecnologie Avanzate II" of the CNR (Rome).

References

1 P. Mazzoldi, G. W. Arnold, G. Battaglin, F. Gonella and R. F. Haglund, Jr., *J. Nonlinear Opt. Phys. Mater.*, 1996, **5**, 285.
2 C. Flytzanis, F. Hache, M. Klein, D. Ricard and P. Roussignol, *Prog. Opt.*, 1991, **29**, 321.
3 G. Fuxi, *J. Non-Cryst. Solids*, 1991, **129**, 299.
4 L. E. Brus, *J. Chem. Phys.*, 1983, **79**, 5566.
5 S. Schmitt-Rink, D. A. B. Miller and D. S. Chemla, *Phys. Rev.*, 1987, **35**, 8113.
6 H. Gleiter, *Adv. Mater.*, 1992, **4**, 474.
7 H. Nasu, K. Tsunetomo, Y. Tokumitsu and Y. Osaka, *Jpn. J. Appl. Phys.*, 1989, **28**, L862.
8 F. Gonella, *Nucl. Instrum. Methods Phys. Res., Sect. B*, 2000, **166–167**, 831 and refs. therein.
9 E. Cattaruzza, *Nucl. Instrum. Methods Phys. Res., Sect. B*, 2000, **169**, 141 and refs. therein.
10 H. Meherzi-Magharoui, M. Dachraoui, S. Belgacem, K. D. Buhre, R. Kunst, P. Cowache and D. Lincot, *Thin Solid Films*, 1996, **288**, 217.
11 M. Ferrari, L. M. Gratton, A. Maddalena, M. Montagna and C. Tosello, *J. Non-Cryst. Solids*, 1995, **191**, 101.
12 D. A. Glocker and S. I. Shah, *Handbook of Thin Film Process Technology*, Institute of Physics Publishing, Bristol, 1995.
13 I. Dekany, L. Nagy, L. Turi and Z. Kiraly, *Langmuir*, 1996, **12**, 3709.
14 F. Gonella and P. Mazzoldi, in *Handbook of Nanostructured Materials and Nanotechnology-Metal Nanocluster Composite Glasses*, Academic Press, San Diego, 2000.
15 G. Hodes, J. Manasen and D. Cahen, *Nature (London)*, 1976, **261**, 403.
16 T. Minami, *J. Non-Cryst. Solids*, 1987, **95–96**, 107.
17 N. Tohge, M. Asuka and T. Minami, *J. Non-Cryst. Solids*, 1992, **147–148**, 652.
18 L. Armelao, M. De Dominicis and R. Bertoncello, *Proceedings of the meeting "Syntheses and Metodologies in Inorganic Chemistry: New Compounds and Materials"*, Bressanone (BZ), Italy 18–21 December 1995, **vol. 6**, p. 172.
19 B. B. Lakshmi, J. Patrissi and C. R. Martin, *Chem. Mater.*, 1997, **9**, 2544.
20 U. Schubert, *J. Chem. Soc., Dalton Trans.*, 1996, 3343.
21 C. J. Brinker and G. W. Scherer, *Sol Gel Science: The Physics and Chemistry of Sol–gel Processing*, Academic Press, San Diego, 1990.
22 J. D. Mackenzie, *J. Non-Cryst. Solids*, 1988, **100**, 162.
23 J. P. Biersack and L. G. Haggmark, *Nucl. Instrum. Methods*, 1980, **174**, 257.
24 A. L. Stepanov, V. A. Zhikharev, D. E. Hole, P. D. Townsend and I. B. Khaibullin, *Nucl. Instrum. Methods Phys. Res., Sect. B*, 2000, **166–167**, 26.
25 H. Hosono and N. Matsunami, *Phys. Rev. B*, 1993, **48**, 13469.
26 M. Strobel, K.-H. Heinig and W. Möller, *Nucl. Instrum. Methods Phys. Res., Sect. B*, 1999, **148**, 104.
27 M. Antonello, G. W. Arnold, G. Battaglin, R. Bertoncello, E. Cattaruzza, P. Colombo, G. Mattei, P. Mazzoldi and F. Trivillin, *J. Mater. Chem.*, 1998, **8**, 457.
28 R. Bertoncello, S. Gross, F. Trivillin, F. Caccavale, E. Cattaruzza, P. Mazzoldi, G. Mattei, G. Battaglin and S. Daolio, *J. Mater. Res.*, 1999, **14**, 2449.
29 L. Armelao, R. Bertoncello and M. De Dominicis, *Adv. Mater.*, 1997, **9**, 736.
30 L. Armelao, P. Colombo, M. Fabrizio, S. Gross and E. Tondello, *J. Mater. Chem.*, 1999, **9**, 2893.
31 R. Bertoncello, F. Trivillin, E. Cattaruzza, P. Mazzoldi, G. W. Arnold, G. Battaglin and M. Catalano, *J. Appl. Phys.*, 1995, **77**, 1294.
32 M. Dubiel, H. Hofmeister, E. Schurig, E. Wendler and W. Wesch, *Nucl. Instrum. Methods Phys. Res., Sect. B*, 2000, **166–167**, 871.
33 R. A. Kant, S. M. Myers and S. T. Picraux, *J. Appl. Phys.*, 1979, **50**, 214.